Available online at www.sciencedirect.com
SCIENCE DIRECT®
International Journal of Solids and Structures 43 (2006) 2279–2298
INTERNATIONAL JOURNAL OF SOLIDS and STRUCTURES
www.elsevier.com/locate/ijsolstr

Numerical simulation and experimental study of Parallel Seismic test for piles

Shu-Tao Liao [a,*], Jian-Hua Tong [b], Cheng-Hao Chen [c], Tsung-Tsong Wu [d]

[a] Department of Civil Engineering, Chung Hua University, Hsinchu 30067, Taiwan, ROC
[b] Department of Computer Science and Information Engineering, Hungkung University, Taichung 400, Taiwan, ROC
[c] Der-Bao Engineering Consultant, Inc., Tainan 700, Taiwan, ROC
[d] Institute of Applied Mechanics, National Taiwan University, Taipei 106, Taiwan, ROC

Received 28 December 2004; received in revised form 19 March 2005
Available online 13 May 2005

Abstract

The theoretical capabilities of the Parallel Seismic (PS) test for determining the length of piles and characterizing possible defects are investigated in this paper. In deriving the theory, a correction factor is proposed in this paper to enhance the accuracy of the prediction. An axisymmetric finite element (FE) model was developed to carry out a series of parametric studies which included the effects of the pile length, the pile-to-borehole distance and the stiffness of surrounding soil. A miniature experiment using an aluminum bar embedded in epoxy prism was also designed and tested in the lab to verify the theory and to demonstrate the use of the correction factor. The results from the experiment and the numerical FE model were also compared to expose the potential of this nondestructive method to in situ application. The model was further modified to simulate the PS test on defective piles with axisymmetric necks and bulges. It can be concluded that the geometric configuration of a pile and the possible significant defect can be characterized with this nondestructive test.

Keywords: Nondestructive test; Pile; Parallel Seismic method; Integrity test

1. Introduction

The importance of assessing the construction quality of a pile foundation has long been recognized. To achieve this goal, various kinds of destructive and nondestructive tests were developed. In this aspect,

* Corresponding author. Tel.: +886 35186757; fax: +886 35372188.
E-mail address: shutao@chu.edu.tw (S.-T. Liao).

0020-7683/$ - see front matter © 2005 Elsevier Ltd. All rights reserved.
doi:10.1016/j.ijsolstr.2005.03.057

nondestructive testing (NDT) was considered to possess high potential for application because it is featured as cost-effective, damage-free, time-saving, and thus can cover the whole population to avoid the disadvantages of sampling (Baker et al., 1991). The primary goal of carrying out a nondestructive test on a pile is the acquisition of the geometric configuration of the pile. This information, describing the detailed geometry of the pile and the embedded defects if they exist, can first be used to evaluate the integrity of the pile and then be served as the input of a subsequent nonlinear finite element analysis to estimate the bearing capacity (or the ultimate strength) of the pile. This philosophy exposes the vast space that NDT can apply in the future. However, all these potential applications rely on the success of NDT in obtaining the detailed geometry of the intact or defective piles (Liao and Roesset, 1997a). Many researchers have been working on the NDT of piles. Most of the tests can be classified into two categories, i.e., (1) reflection and (2) direct transmission methods. Among them some commonly used examples are Impulse Response (IR) (Davis, 2003; Finno and Gassman, 1998) or Transient Dynamic Response (TDR) (D5882 of ASTM, 2004; Davis and Dunn, 1974), Sonic Echo (SE) (Rausche et al., 1991), Impedance Log (IL) (Paquet, 1991; Rix et al., 1993) and Impact Echo (IE) (Lin et al., 1997; Sadri and Afshin, 2003) tests as categorized in reflection methods and Cross-hole Sonic Logging (CSL) and Parallel Seismic (PS) (Olson et al., 1995) tests as categorized in direct transmission methods. In reflection methods, the force to introduce a disturbance to a pile and the receiver to collect the response of the pile are basically applied at the pile head, whereas in direct transmission methods the receiver is placed at intervals in a tube or borehole which must be cored or drilled before testing. Therefore reflection methods are in general faster and more cost-effective. However, direct transmission methods can obtain the information in a more direct way and they can be applied to piles with much larger length.

Among the reflection methods, Lin et al. (1997) used the IE tests to successfully detect the lengths of piles and the depths of the embedded necks. Using the finite element method, Liao and Roesset (1997b) developed one, two, and three-dimensional models to simulate the IR test for intact piles. A series of parametric studies were carried out to demonstrate the capabilities of this method in determining the lengths and cross sectional areas of intact piles under various kinds of soil conditions. The numerical models of IR tests were later extended to study piles with axisymmetric irregularities such as necks and bulges. The results indicated that by analyzing the mechanical admittance (or mobility) curves, the depth and length of the necks (or bulges) can be determined in good precision. However, the methodology to determine the widths of the defects seems to remain pending. The results of this paper primarily indicated that this goal can be achieved by the PS test, which has not been thoroughly studied due to limited application for its relatively high cost of operation. However, this method plays an important role in the second line for settling down the dispute on suspicious yet critical piles. This paper will also propose a correction factor to be incorporated in the traditional procedure of this method to enhance the accuracy of the estimation on the length of piles.

The determination of the substantial length of a pile exhibits a high value in practical application, particularly when evaluating the integrity of existing foundations such as piles with cap. This point can be illustrated with an engineering problem arose after the disastrous earthquake, the Ji-Ji Earthquake, struck central Taiwan on September 21, 1999. A lot of structures were damaged or collapsed in the attack. The post-earthquake evaluation on the integrity of the structures played an important role in the success of the later retrofitting work. In this aspect, the integrity evaluation of the existing foundations is among the most difficult. Shown in Fig. 1 is the in-built bridge system of a superhighway near central Taiwan. To the time when the earthquake struck, the supporting system of the bridge had just been finished as shown in the picture. There was no problem for the engineers to make the decision to replace the superstructure of the system as the huge damages being discovered in the inspection. However, the difficult situation was to determine how seriously the foundations were damaged and whether the supporting piles should be replaced. To settle down this problem, a painful decision was made to carry out the coring test on some piles. The sampling rate is 28 out of 350 piles in the region. Most of the cored cylinders are concrete until a depth of 13 m and soil beyond the depth. The designed length of the piles is 25 m and this result

Fig. 1. In-built bridge system of a superhighway in central Taiwan. (Photo courtesy of Taiwan Area National Expressway Engineering Bureau.)

indicated that the piles were twisted seriously to break at about the mid-height, as shown in Fig. 2. As a matter of fact, this conclusion can be reached in a much safer and economic way if the substantial length of the piles can be obtained with nondestructive testing methods. The goal of this kind of applications may be summarized to the determination of the substantial length of single piles, or much more difficult cases,

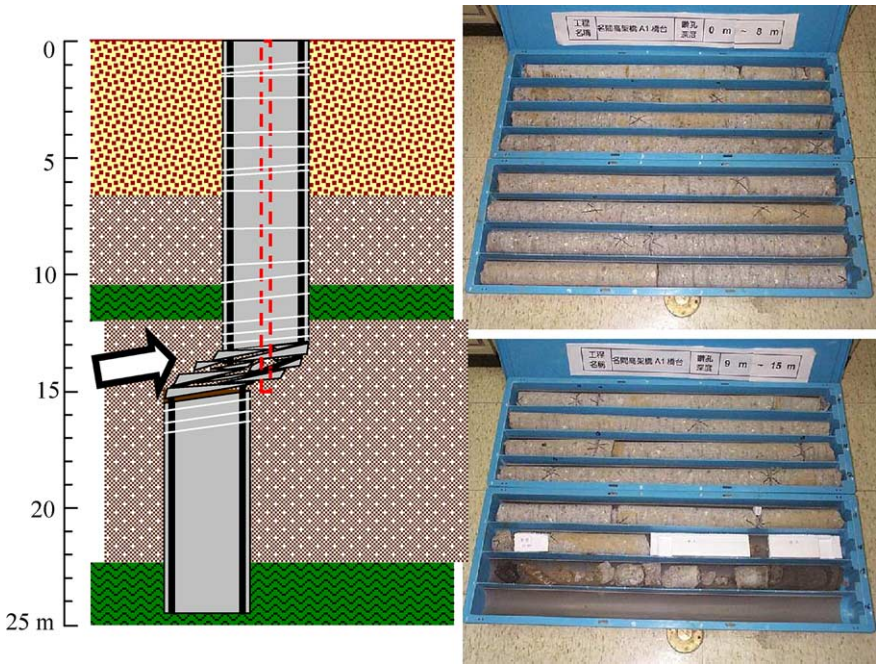

Fig. 2. Cored cylinders indicating the break of piles. (Photo courtesy of Taiwan Area National Expressway Engineering Bureau.)

piles with cap. To reach this goal, all the tools such as the Parallel Seismic method should attract deeper study than before.

2. Regular procedure of Parallel Seismic test

In Parallel Seismic tests, the top or side of the pile is struck by an instrumented hammer and the propagated stress wave is sensed by a hydrophone placed in a cased, water-filled borehole drilled next to the pile (Olson et al., 1995). As schematically shown in Fig. 3, the receivers are placed at different depths along the borehole to record the time histories of the motion caused by the induced stress waves. As an example, Fig. 4 shows the velocity time history sensed by a receiver. The time of the first arrival of the P wave, defined as the earliest time when the response curve starts to fluctuate, is then identified from the waveform. For each receiver this arrival time, as marked with "T_0" in Fig. 4, is plotted versus the depth of the corresponding receiver on an x–y plot, as shown in Fig. 5 (Liao et al., 1998). Usually the data points can be grouped into two families and approximately fitted by two straight lines. The y-coordinate, i.e, the depth, of their intersection point indicates the length of the pile. The theoretical background of this regular procedure will be explored in the next section to verify the validity of this method. In doing so, a correction factor to enhance the accuracy of this method can be concluded.

3. Theoretical derivation and correction factor

Consider a pile partially or fully embedded in soil, as shown in Fig. 6. The pile system consists of a column, which is assumed to be made of concrete, and the soil. The pile has a circular cross-sectional area with a radius r. The length of the pile above the ground is denoted by L_A and the total length is L. The distance between the lateral surface of the pile and the receiver borehole is denoted by D. An external impact is

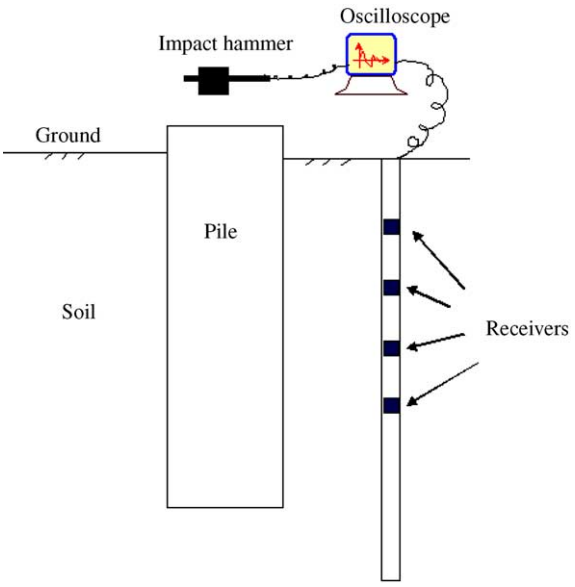

Fig. 3. Parallel Seismic test for a pile.

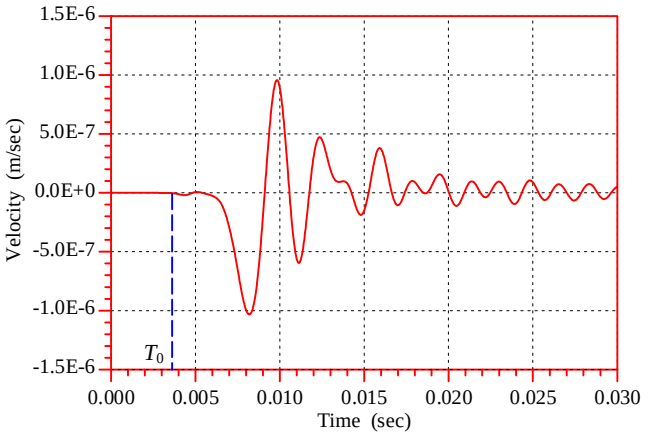

Fig. 4. Identification of first arrival time of stress wave from velocity time history.

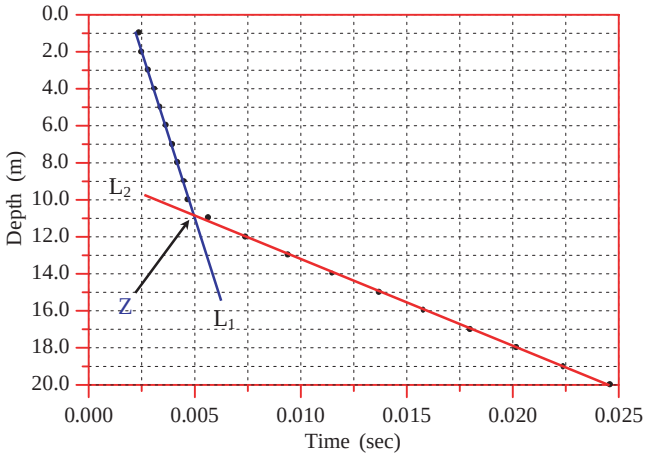

Fig. 5. Determination of pile length from depth-versus-time plot in PS test.

applied at the center of the top surface of the pile. The contact area is relatively small compared to the cross sectional area of the pile so that the impact may be treated as a point source. The receivers in the borehole can be categorized into two groups based on whether the receiver is located above or below the level of the pile bottom. Let H_1 denote the distance between the level of the pile head and a receiver B_1 which belongs to the first group. Using the ray path theory a stress wave is assumed to start from the center of the loaded area O, passing through a point A_1, which is located at the lateral surface of the pile, and arriving at the receiver B_1. Let S_1 denote the travel length of this path $O \to A_1 \to B_1$. Let V_1 and V_2 denote the propagation velocities of the waves in pile and soil, respectively. The refraction at the interface of the pile and the surrounding soil should obey Snell's law, which states that $\sin\theta_1/V_1 = \sin\theta_2/V_2$ where θ_1 and θ_2 denote the angles between the normal vector of the interface and the ray paths in the two media. Then,

$$S_1 = \sqrt{(H_1 - X)^2 + r^2} + \sqrt{D^2 + X^2} = (H_1 - X)\sqrt{1 + \left(\frac{r}{H_1 - X}\right)^2} + \sqrt{D^2 + X^2} \tag{1}$$

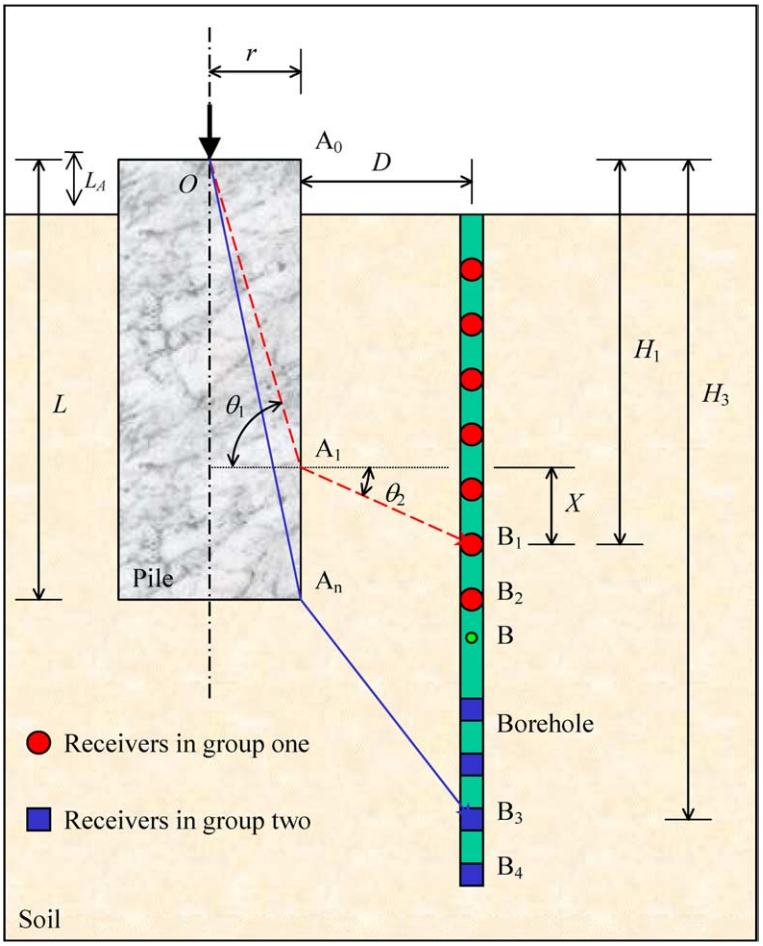

Fig. 6. Traveling paths of stress waves in a Parallel Seismic test.

where

$$X = D \cdot \tan\theta_2 \tag{2}$$

$$\theta_2 = \sin^{-1}\left(\sin\theta_1 \cdot \frac{V_2}{V_1}\right) \tag{3}$$

In the case where $(H_1 - X) \gg r$, Eq. (1) becomes

$$S_1 \approx (H_1 - X) + \sqrt{D^2 + X^2} = (H_1 - X) + F \tag{4}$$

where

$$F = \sqrt{D^2 + X^2} \tag{5}$$

Thus the total travel time T_1 for the P wave to propagate through the path S_1 and then arrive at B_1 would be

$$T_1 = \frac{(H_1 - X)}{V_1} + \frac{F}{V_2} \tag{6}$$

Referring to the arrival time versus depth plot as shown in Fig. 5, the equation of the straight line L_1 which is selected to represent the data points of the first group can be given as follows:

$$L_1 : T = \frac{(H - X)}{V_1} + \frac{F}{V_2} \tag{7}$$

In the same manner, let H_3 denote the distance between the level of the pile head and a receiver B_3 which is placed at a large depth and belongs to the second group. The travel distance S_3 of the path $O \rightarrow A_n \rightarrow B_3$ would be

$$S_3 = \sqrt{L^2 + r^2} + \sqrt{D^2 + (H_3 - L)^2} = L\sqrt{1 + \left(\frac{r}{L}\right)^2} + (H_3 - L)\sqrt{1 + \left(\frac{D}{H_3 - L}\right)^2} \tag{8}$$

In the general cases where $(H_3 - L) \gg D$ and $L \gg r$, S_3 can be approximated by

$$S_3 \approx L + (H_3 - L) \tag{9}$$

Therefore the travel time T_3 associated with S_3 would be

$$T_3 = \frac{L}{V_1} + \frac{(H_3 - L)}{V_2}$$

The equation of the straight line L_2 for the second group in Fig. 5 can thus be given by

$$L_2 : T = \frac{L}{V_1} + \frac{(H - L)}{V_2} \tag{10}$$

Let H_I denote the depth of the receiver associated with the intersection point of the two lines L_1 and L_2, solving Eqs. (7) and (10) may reach

$$H_I = L + \frac{V_1}{V_1 - V_2}F - \frac{V_2}{V_1 - V_2}X \tag{11}$$

That is,

$$L = H_I - R \tag{12}$$

where

$$R = \frac{V_1}{V_1 - V_2}F - \frac{V_2}{V_1 - V_2}X \tag{13}$$

is defined as the correction factor in this paper. In comparison with the conventional strategy which approximates the length of the pile with H_I, it will be shown later that the accuracy in predicting the true length L of the pile can be enhanced when the correction factor R is taken into account.

4. Finite element model

An axisymmetric finite element model was used to model the pile and the surrounding soil as shown in Fig. 7. The complete domain of the problem can be obtained by rotating this figure about the centerline of the pile. The four-noded, quadrilateral, and isoparametric (Q4) element was selected to use in this model. After discretization, the equations of motion in matrix form for finite analysis can be obtained. The central difference scheme was then adopted to carry out the integration for the equations of motion to obtain the

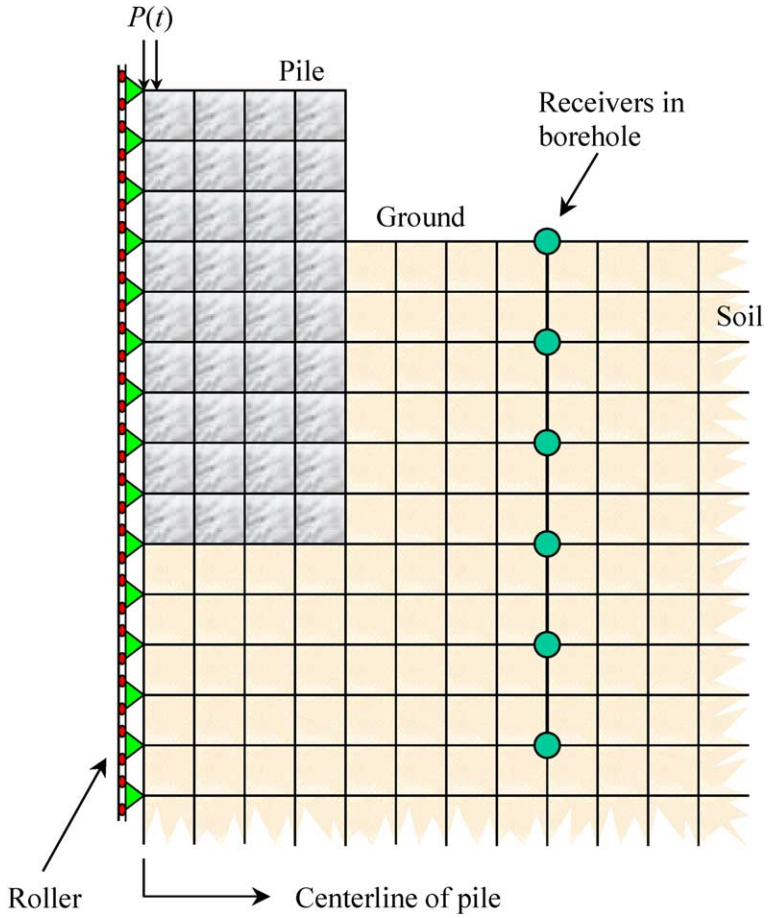

Fig. 7. Axisymmetric finite element model for the PS test of a pile.

nodal displacements at each time step (Liao and Roesset, 1997b). It should be noted that the central difference method is conditionally stable so that for stability, the time step Δt should be smaller than a critical value, Δt_{cr}, which is controlled by the maximum natural frequency (or minimum natural period) of the finite elements for the system. A program was developed to implement the direct iteration scheme to determine the value of Δt_{cr}.

The loading pressure $P(t)$ used in this paper was defined as a function of time by

$$P(t) = P_0 \sin \bar{\omega} t \quad \text{for } 0 \leqslant t \leqslant T_d \tag{14}$$

and $P(t) = 0$ for $t > T_d$ where $\bar{\omega} = \pi / T_d$. This represents a sinusoidal impact of half a cycle duration with a period of $2T_d$. In this paper, $T_d = 1.5$ ms $= 1.5 \times 10^{-3}$ s and $P_0 = 15{,}570$ N/m^2. The radius of the loaded area is set at $r_L = 0.0254$ m.

5. Experimental verification

To verify the capability of the PS method in determining the length of the pile and to evaluate the potential of the correction factor in enhancing the accuracy of estimation, a miniature experiment was

carried out in the laboratory. The experimental results will be also compared to those obtained with the finite element simulation so that the numerical model can be verified for later use in parametric study.

5.1. Experimental results

Consider an aluminum cylinder embedded in an epoxy bulk, as shown in Fig. 8. The height of the epoxy prism is 38 cm. The dimension of the square cross section of this prism is 8 cm by 8 cm. The radius and the total length of the aluminum bar are 1.3 cm and 31 cm, respectively. The length of the bar above the top level of the epoxy prism is 4 cm. The axis of the bar coincides with the center line of the prism. The Young's modulus E_{Al}, Poisson's ratio v_{Al}, and mass density ρ_{Al} of the aluminum bar are provided in Table 1. The propagation velocities of the P (primary) and S (shear) waves, denoted by $V_{\mathrm{Al\text{-}P}}$ and $V_{\mathrm{Al\text{-}S}}$, are also listed in the table. In the table, the theoretical velocities of P and S waves propagating in a material were calculated by

$$V_{\mathrm{P}} = \sqrt{\frac{(1-v)E}{(1+v)(1-2v)\rho}} \tag{15}$$

$$V_{\mathrm{S}} = \sqrt{\frac{G}{\rho}} = \sqrt{\frac{E}{2(1+v)\rho}} \tag{16}$$

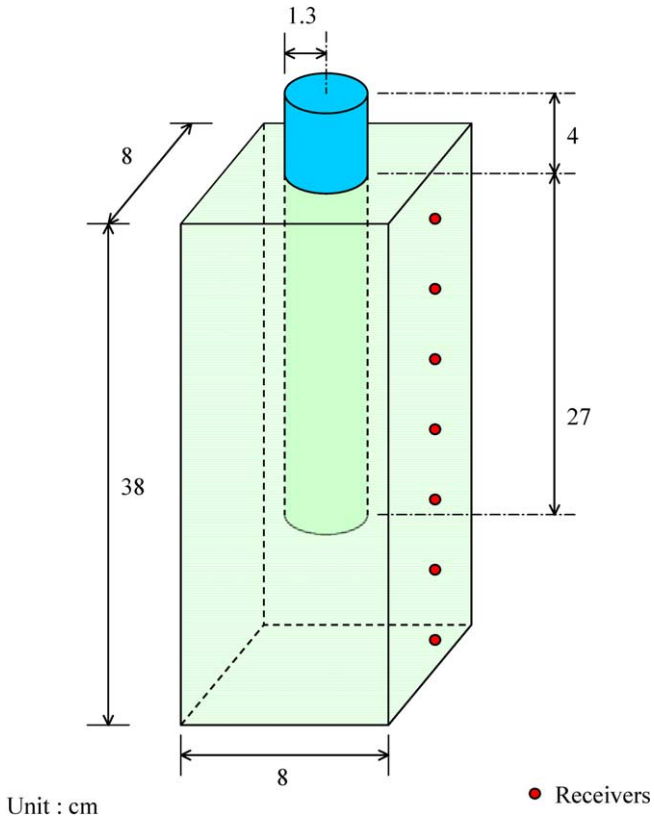

Fig. 8. Geometric configuration of the experimental model for a PS test.

Table 1
Material properties of aluminum bar and epoxy prism and the corresponding stress wave velocities

	Aluminum bar	Epoxy prism
Young's modulus (N/m^2)	7.24×10^{10}	3.94×10^9
Poisson's ratio	0.35	0.38
Mass density (kg/m^3)	2800	1160
P wave velocity (m/s)	6390	2500
S wave velocity (m/s)	3100	1110

where G is the shear modulus of the material. For comparison purpose, the Young's modulus E_{E_p}, Poisson's ratio v_{E_p}, and mass density ρ_{E_p} of the epoxy bulk, as well as the P and S wave velocities, $V_{E_p\text{-}P}$ and $V_{E_p\text{-}S}$, are also provided in the table. It can be seen that the ratio of the P wave velocities in aluminum and epoxy is about 2.6, a number much lower than that of those in concrete (Wu and Fang, 1997) and normal soil, which is about 9. This condition places the outcome on a conservative side since now it is more difficult to determine the length of the aluminum bar in the laboratory condition than the length of a concrete pile in practical site with the PS method.

An impact was introduced by triggering the falling of a small steel ball at the center of the top surface of the aluminum bar. In this study, a laboratory-built vertically polarized conical transducer (Tong et al., 2002) was utilized to measure the vertical component of the surface displacement signals. The received voltage signal from the conical transducer was amplified by a preamplifier and recorded by a 100 MHz digital oscilloscope (LeCroy 9314L) (Tong et al., 2001). It is noted that the preamplifier must be embedded in the transducer assembly to minimize the electric noise. The first receiver was placed 10 cm down from the top level of the aluminum bar at the side surface of the epoxy prism, as shown in Fig. 8. Then the receiver was moved down at the side surface of the epoxy prism at an interval of 5 cm until 40 cm deep down from the top level of the aluminum bar. The displacement amplitude recorded at the first receiver, which is placed at 10 cm down from the top level of the aluminum bar, is presented in Fig. 9 as a function of time. The next step in the PS method is to identify the arrival time of the first P wave from this response curve. However, this work can be done more easily and accurately from velocity time history because it is sharper. The direct way to get the velocity is to obtain the time derivative of the displacement. However, the high-frequency fluctuations resulted from in situ noises and the digitalization of the data may cause a problem in obtaining

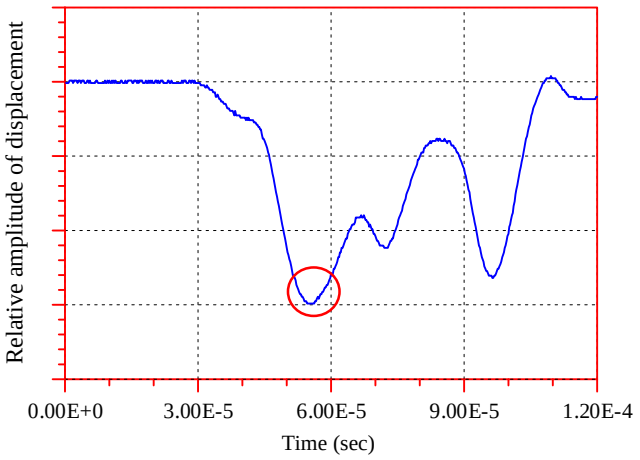

Fig. 9. Original displacement amplitude obtained at 10 cm from the bar head in experiment.

this derivative. This phenomenon can be seen as the circled part in the curve of Fig. 9 is blown up and presented by a dashed line in Fig. 10. Using the Moving Average (MA) method to manipulate the original displacement, a much smooth curve can be obtained as shown in the figure with a solid line. Based on this smooth displacement, the corresponding velocity time history was obtained and presented by the dashed curve in Fig. 11. Similarly, the velocity recorded at the side surface of the epoxy prism at the distances of 20 cm down from the top level of the aluminum bar is plotted as the dashed curves in Fig. 12. The next step in the PS method is to identify the arrival times of the first P waves in each figure and then plot the depth-to-arrival-time curve for determining the length of the aluminum bar. This result is presented in Fig. 13. The arrival time of the first P wave is identified by comparing the signal and an undisturbed datum line (Tong et al., 2002). In Fig. 13, data points A and B are then selected to form the first straight line and points C and D, the second. The intersection point of these two lines indicates that the length of the bar is 33.6 cm, as predicted with the regular procedure of the PS method. The error is 8.4% since the true length of

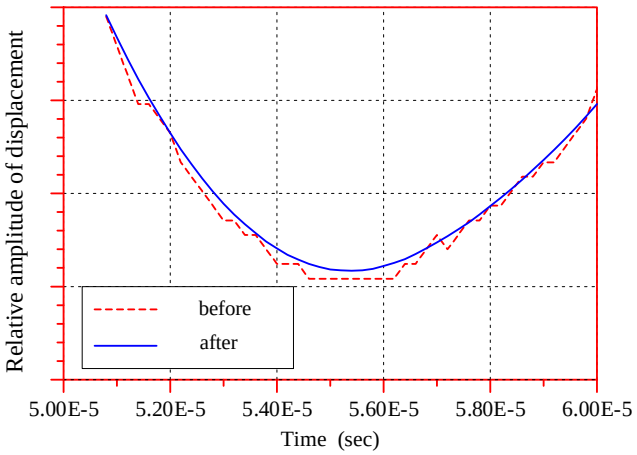

Fig. 10. Displacement amplitude before and after the processing of moving average scheme.

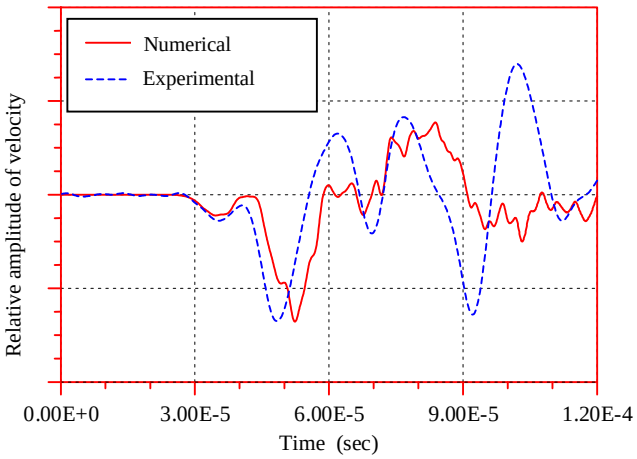

Fig. 11. Comparison of numerical and experimental results in velocity obtained at 10 cm from bar head.

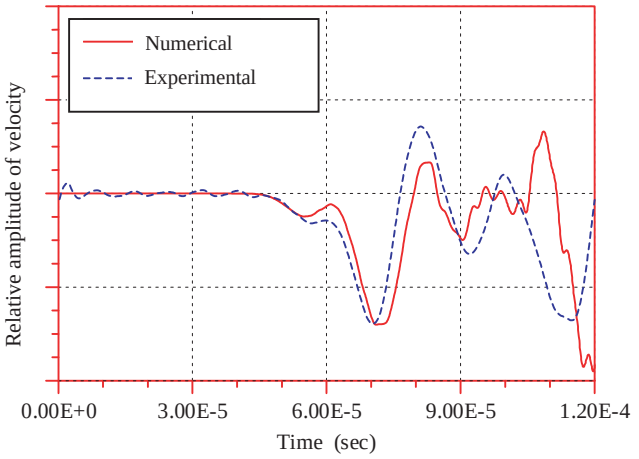

Fig. 12. Comparison of numerical and experimental results in velocity obtained at 20 cm from bar head.

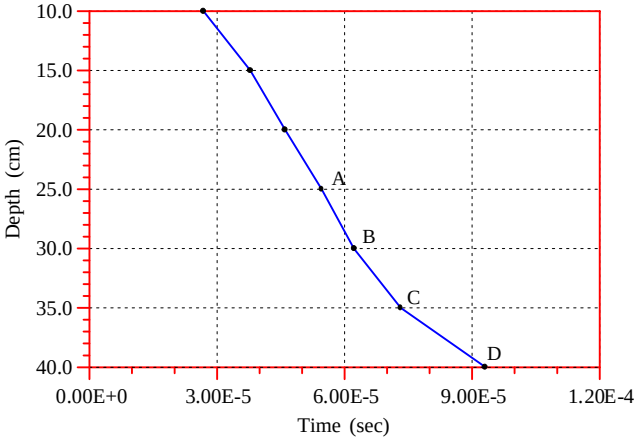

Fig. 13. Experimental results of the aluminum bar model in depth-versus-time plot.

the bar is 31 cm. However as the correction factor, which is calculated to be $R = 3.9$ cm, is taken into account, the predicted length is modified to be 29.7 cm, which is only 4.2% in error.

5.2. Comparison of numerical and experimental results

To cultivate a numerical model for the use of parametric study for this research, the finite element model developed and introduced in this paper was used to simulate the PS test carried out in the lab as mentioned above. The system for the numerical model to simulate is shown in Fig. 14. It is noted that the epoxy prism shown in Fig. 8 as for the experiment is now replaced by an epoxy cylinder with a diameter of 8 cm because the finite element model to be used is axisymmetric. This modification, which resulted from the limitation of the developed finite element model, surely will affect the comparableness of the results with those obtained from the experiment. However, the effect is expected to be small because of this small discrepancy on the

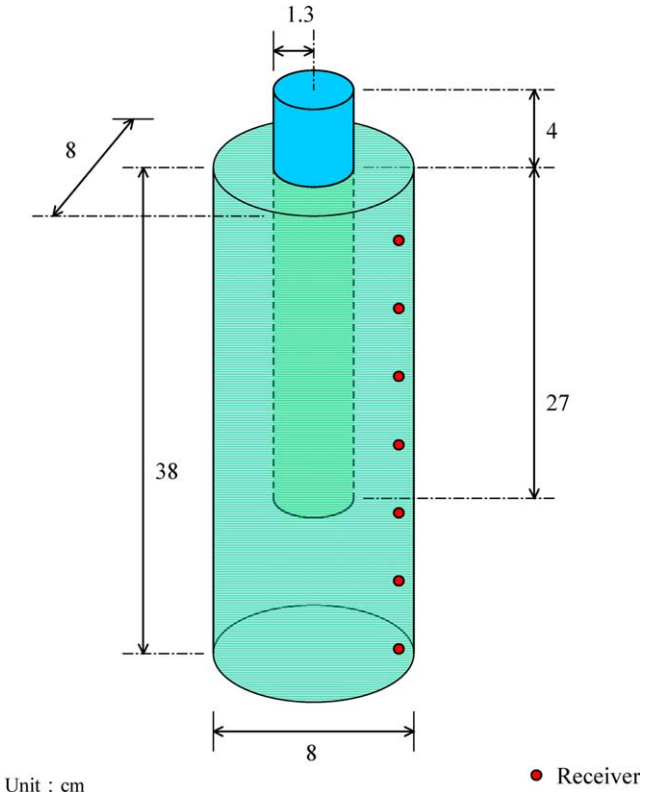

Fig. 14. Geometric configuration of numerical model for simulating the experiment.

boundary condition. Furthermore, what matter in a PS test are the arrival times of the first P waves at the receivers. The simulation results of the finite element model are then plotted together with those from the experiment. The velocity time histories at the receivers located at distances of 10 and 20 cm down from

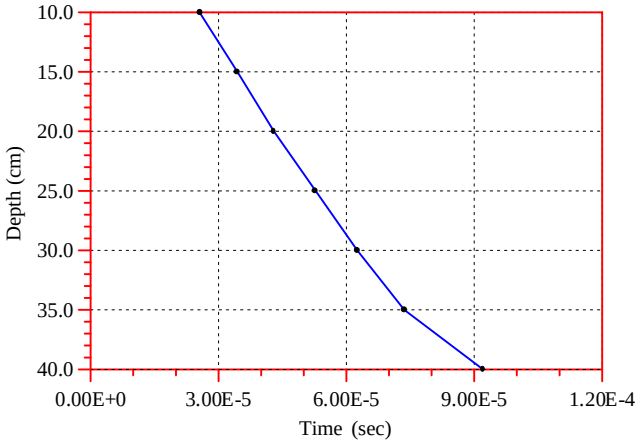

Fig. 15. Results of numerical simulation for the experiment in depth-versus-time plot.

the top level of the aluminum bar are plotted with the solid curves in Figs. 11 and 12, respectively. It is very easy to note that the results from the numerical model match well with those from the experiment at the initial stage and then the accordance deteriorates with time, as expected. The arrival times of the first P waves in each figure are then identified to plot the depth-versus-arrival-time curve, as shown in Fig. 15. Two straight lines can easily be defined to fit these data points and their intersection point indicates that the length of the bar is 34.2 cm, using the regular procedure of the PS method. The error is 10.3% since the true length of the bar is 31 cm. However as the correction factor is taken into account, the predicted length is modified to be 30.3 cm, which is only 2.3% in error. Comparing Figs. 15 and 13 reveals that forming the two straight lines is even more straightforward for the numerical than experimental results. And also the prediction error is even smaller.

6. Parametric studies on intact piles

Once the validity of the developed finite element model had been verified with the experimental results, a series of parametric studies were then carried out to study the capability of the PS tests and the proposed correction factor. The parameters to be varied include pile length, pile to borehole distance, and soil stiffness. Referring to Fig. 6, consider an intact pile with a total length of $L = 12$ m. The pile has a circular cross-sectional area with a radius $r = 0.5$ m. The lengths of the pile above and below ground are 1 and 11 m, respectively. The material properties of the soil and the concrete pile are given in Table 2, in which E_c, v_c, ρ_c and E_s, v_s, ρ_s are the Young's modulus, Poisson's ratio, and mass density of the concrete pile and surrounding soil. The theoretical wave velocities of P and S waves in the concrete and soil are also calculated with Eqs. (15) and (16) and provided in the table. The pile-to-borehole distance D is set at 1 m. The receiver is lowered into the borehole and takes the measurements in velocity at an interval of 1 meter until a depth of 19 m from the ground (or 20 m from the top level of the pile).

6.1. Effect of correction factor

Consider the example mentioned above. The measurements of the particle velocity in the vertical direction were made at an interval of 1 m down along the receiver borehole. Using the finite element model, the velocity response at the depths of 12 m from the pile head is presented for example in Fig. 16. The first arrivals of the P waves are selected directly from the finite element results and marked with "PP" in the figures. The approximate times of arrival of the waves which travel with the P wave in the pile and then the S wave in the soil are marked with "PS" in the figures for reference. The depths versus the arrival times are plotted in Fig. 17. The two data points (marked with "A" and "B" in the figure) associated with 11 and 12 m depth are chosen to define the first straight line and points 19 and 20 (marked with "C" and "D") are chosen to define the second. After calculation, the depth of the intersection of these two straight lines is $H_I = 12.95$ m, based on the conventional procedure of the Parallel Seismic test. The error is 7.9%. Using

Table 2
Concrete and soil properties and corresponding wave velocities

Concrete		Soil		Unit
E_c	3.31×10^{10}	E_s	1.8×10^8	N/m^2
ρ_c	2300	ρ_s	1925	kg/m^3
v_c	0.2	v_s	0.4	
V_P	4000	V_P	450	m/s
V_S	2450	V_S	183	m/s

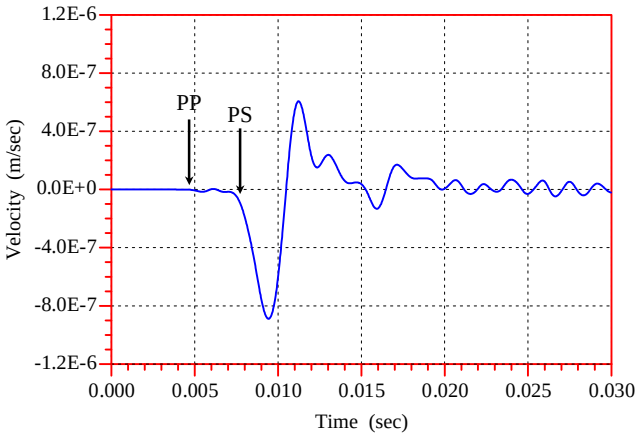

Fig. 16. Velocity response of intact pile to the PS test obtained at 10 m from pile head.

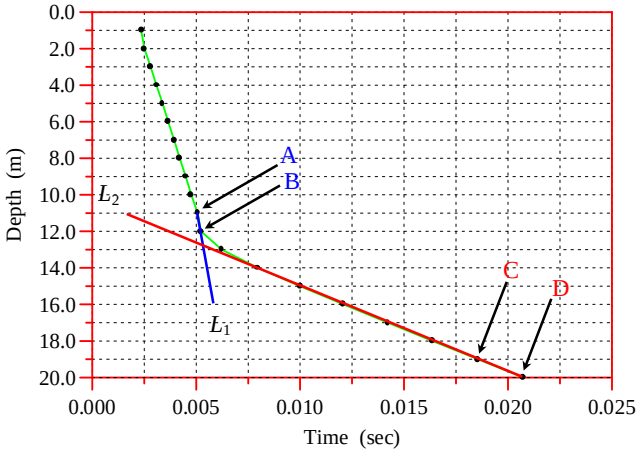

Fig. 17. Depth-versus-time plot of example intact pile to the PS test.

Eqs. (3), (2), (5) and (13), the value of the correction factor for this case can be calculated to be 1.12 m. Thus the length of the pile is recovered to be

$$L = H - R = 12.95 - 1.12 = 11.83$$

The error is now reduced from 7.9% to 1.4%.

6.2. Effect of pile length

To examine the capability of the correction factor, the embedded length of the pile is first decreased from 11 m to 9 and 10 m and then increased to 12 and 13 m so that the total length of the pile is 10 to 14 m. The results are presented in the depth versus arrival time plot as shown in Fig. 18. The results before and after taking the correction factor into account are presented in Table 3. The error in predicting the total length of the pile with the conventional procedure decreases from 10.3% to 6.5% as the length of the pile increases. After taking the correction factor into account, the errors for all cases are within 1.5%.

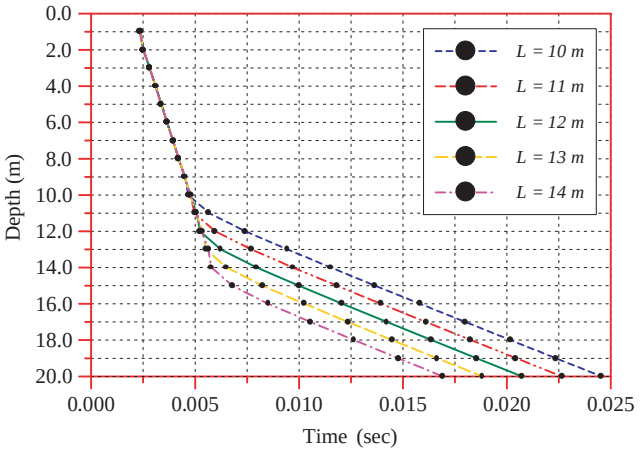

Fig. 18. Depth-versus-time plot of intact piles with lengths of 10, 11, 12, 13, and 14 m.

Table 3
Estimation and error of length prediction for piles with different lengths

	Pile length, L (m)				
	10	11	12	13	14
Initial estimate, Z (m)	11.03	12.04	12.95	13.98	14.91
Error %	10.3	9.5	7.9	7.5	6.5
Correction factor, R (m)	1.12	1.12	1.12	1.12	1.12
Modified length, L (m)	9.91	10.92	11.83	12.86	13.79
Error %	0.9	0.7	1.4	1.1	1.5

6.3. Effect of pile-to-borehole distance

The distance between the receiver borehole and the lateral surface of the pile is now increased from $D = 1$ m to 1.5, 2.0, 2.5, and 3 m. The results are presented in Fig. 19 and summarized in Table 4. It can be seen that the error in predicting the total length of the pile increases as the distance between the borehole and the pile increases. This error increases from about 8% for $D = 1$ m to 20% for $D = 3$ m if conventional procedure is used. The errors are about 1.4–8.2% if the correction factors are taken into account. The trend that the error increases as D increases can be expected in deriving the correction factor where $(H - L)$ was assumed to be far greater than D.

6.4. Effect of soil stiffness

To study the effect of soil stiffness, the Young's modulus of the soil E_s is increased so that the P wave velocity in the soil is increased from $V_P = 450$ to 1350, 2250, 3150, and 4050 m/s. In other words, the ratio of the P wave velocities in the pile and soil is decreased from 8.9 to 3.0, 1.8, 1.3, and 1.0. The results are presented in Fig. 20 and summarized in Table 5. The figure indicates that determining the intersection point becomes harder as the stiffness of the soil increases toward that of the pile. In the cases where the ratio of the P wave velocities in the pile and soil is less than 2, it is unpractical to predict the length of the pile with this method. As shown in Table 5, the error in predicting the length of the pile ranges is about 8–16% and 1–8% before and after using the correction factor.

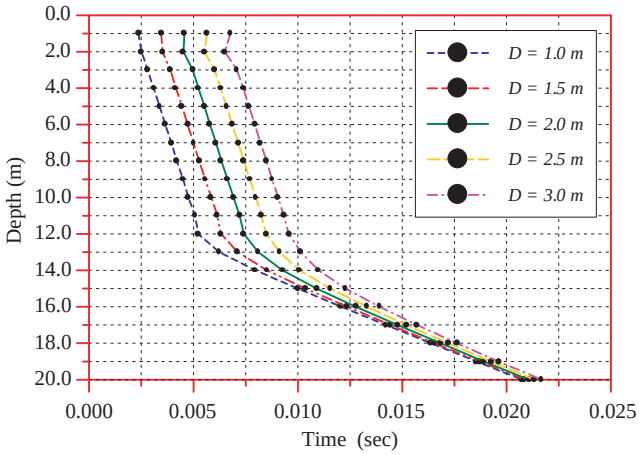

Fig. 19. Depth-versus-time plot of intact piles with pile-to-borehole distances of 1, 1.5, 2, 2.5, and 3 m.

Table 4
Estimation and error of length prediction for piles with different pile-to-borehole distances

	Pile-to-borehole distance, D				
	1.0	1.5	2.0	2.5	3.0
Initial estimate, Z (m)	12.95	13.38	13.78	14.06	14.38
Error %	7.9	11.5	14.8	17.2	19.8
Correction factor, R (m)	1.12	1.68	2.24	2.79	3.36
Modified length, L (m)	11.83	11.70	11.54	11.27	11.02
Error %	1.4	2.5	3.8	6.1	8.2

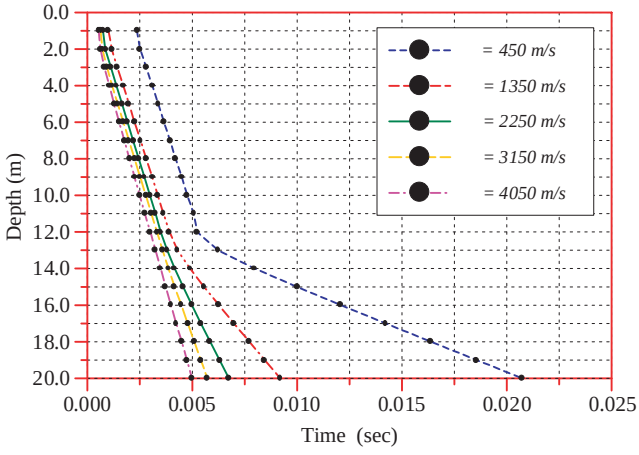

Fig. 20. Depth-versus-time plot of intact piles in soil with P wave velocities being 450, 1350, 2250, 3150, and 4050 m/s.

Table 5
Estimation and error of length prediction for pile systems with different wave velocities in soil

	P wave velocity, V_P				
	450	1350	2250	3150	4050
Initial estimate, Z (m)	12.95	13.35	13.56	13.93	12.91
Error %	7.94	11.22	12.96	16.10	7.58
Correction factor, R (m)	1.12	1.42	1.89	2.87	NA
Modified length, L (m)	11.83	11.93	11.67	11.06	NA
Error %	1.39	0.60	2.72	7.80	NA

7. Numerical simulation on defective piles

To study the capability of the PS method in identifying and quantifying the defects embedded in piles, the finite element model was used to simulate the response of defective piles. Two kinds of defects were considered. They are axisymmetric neck and bulge, which result in a reduction and expansion in the cross sectional area of a pile, respectively.

7.1. Pile with axisymmetric neck

Consider the intact pile discussed in previous section. Now a neck is introduced into the pile at a distance between 5 m and 8 m from the pile head. The original radius of the pile is 0.5 m. To study the effect of a neck in the response of a pile to the PS test, consider that the radius of the pile in the range of the neck is reduced to $F_r = 0.4$, 0.3, 0.2, and 0.1 m, respectively. The depth versus arrival time curve of these PS tests is presented in Fig. 21. It can be seen in all defective cases that a neck results in a delay in the arrival time and thus the data points associated with the defective area deviate to the right from the original straight line. Furthermore, the deviation becomes larger as the neck-in becomes worse. The arrival times will go back to the original straight lines as the depth of the receivers goes deeper than the neck. In other words, the depth, the extent as well as the thickness of the neck can be characterized from the result of a PS test, at least in theoretical sense.

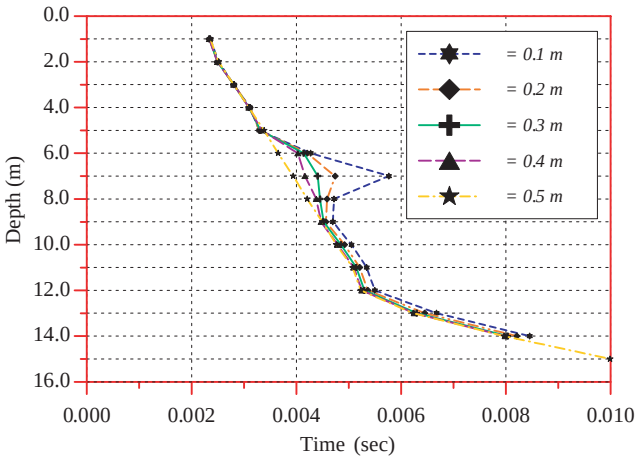

Fig. 21. Depth-versus-time plot of intact and defective piles with radius of pile in neck area being 0.1, 0.2, 0.3, 0.4, and 0.5 m.

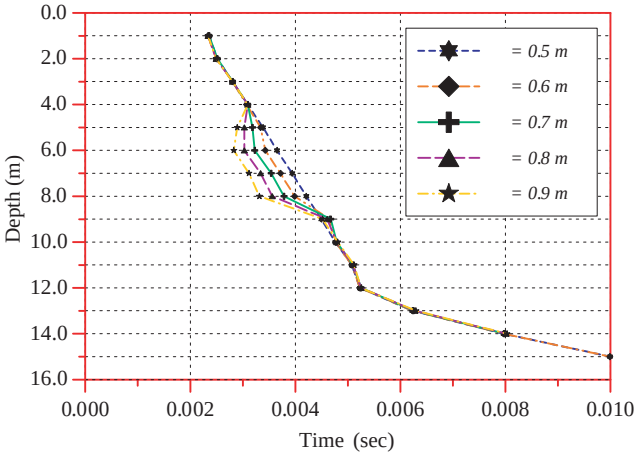

Fig. 22. Depth-versus-time plot of intact and defective piles with radius of pile in bulge area being 0.5, 0.6, 0.7, 0.8, and 0.9 m.

7.2. Pile with axisymmetric bulge

Next consider that the neck discussed above is replaced by a bulge. For comparison purpose, the radius of the pile in the range of the bulge is increased from the normal one, $F_r = 0.5$ m, to 0.6, 0.7, 0.8, and 0.9 m, respectively. The depth versus arrival time curve is presented in Fig. 22. To the contrary, a bulge results in an early arrival of the stress wave and thus the data points associated with the bulge area deviate to the left from the original straight line. Furthermore, the deviation increases with the radius of the bulge. Therefore, it is feasible to identify the depth, the extent and the thickness of the bulge through the PS test.

8. Conclusions

The potential of the Parallel Seismic test in determining the length of the pile and locating a possible defect as a neck or bulge is evaluated in this paper. A correction factor is proposed to be incorporated into the regular procedure of the method in recovering the length of the pile. The results indicated that the accuracy in predicting the length of the pile can be effectively enhanced when the correction factor is taken into account. A miniature experiment was designed and carried out to verify the feasibility of this method and to demonstrate the effectiveness of this correction factor. The results from the experiment indicated that the error in predicting the bar length with the PS method can be reduced from 8.4% as with the traditional procedure to 4.2% as the correction factor being taken into account. An axisymmetric finite element model developed for simulating the PS test was used to cross check with the experimental results. With this numerical model, a series of parametric studies were carried out to study the effects of these parameters in the accuracy of prediction. From the study, it is concluded that the error of the estimate increases with the pile-to- borehole distance but decreases with the pile length. In all cases, the correction factor plays a good role in enhancing the accuracy of the estimation. Another observation is that the predicting work becomes harder as the stiffness of the surrounding soil increases toward that of the pile. The numerical model was finally used to simulate the response of a defective pile with a neck or bulge. The results indicated that the capability of the PS method in locating and characterizing the neck or bulge is promising.

Acknowledgments

The work presented in this paper was financially supported by the National Science Council of Taiwan, ROC, under the grants NSC89-2625-Z-216-002 and NSC90-2211-E-216-006. These helps are gratefully acknowledged.

References

ASTM Book of Standards, 2004. D5882, vol. 04.09.

Baker Jr., C.N., Drumright, E.E., Mensah, F.D., Parikh, G., Ealy, C.D., 1991. Use of nondestructive testing to evaluate defects in drilled shafts: results of FHWA research. Integrity Testing of Foundations, Transportation Research Record 1331, 28–35.

Davis, A.G., 2003. The nondestructive impulse response test in North America: 1985–2001. NDT & E International 36, 185–193.

Davis, A.G., Dunn, C.S., 1974. From theory to filed experience with the nondestructive vibration testing of piles. Proceedings of the Institution of Civil Engineers, Part 2, 571–593.

Finno, R.J., Gassman, S.L., 1998. Impulse response evaluation of drilled shafts. Journal of Geotechnical and Environmental Engineering, ASCE 124 (10), 965–975.

Liao, S.-T., Roesset, J.M., 1997a. Identification of defects in piles through dynamic testing. International Journal for Numerical and Analytical Methods in Geomechanics 21 (4), 277–291.

Liao, S.-T., Roesset, J.M., 1997b. Dynamic response of intact piles to impulse loads. International Journal for Numerical and Analytical Methods in Geomechanics 21 (4), 255–275.

Liao, S.-T., Roesset, J.M., Chen, C.-H., 1998. Numerical simulation of nondestructive Parallel Seismic test for piles. In: The Sixth East Asia-Pacific Conference on Structural Engineering and Construction, Taipei, Taiwan, 1997–2003.

Lin, Y., Sansalone, M., Carino, N.J., 1997. Impact-echo response of concrete shafts. Geotechnical Testing Journal 14 (2), 121–137.

Olson, L.D., Jalinoos, F., Aouad, M.F., 1995. Determination of Unknown Subsurface Bridge Foundations, Report submitted to NCHRP, Transportation Research Board, National Research Council, pp. 129–148.

Paquet, J., 1991. A new method for testing integrity of piles by dynamic impulse: the impedance log. International Colloquium on Deep Foundations, Paris, March, pp. 1–10.

Rausche, F., Shen, R.K., Likins Jr., G.E., 1991. Comparison of pulse echo and transient response pile integrity test methods. Integrity Testing of Foundations, Transportation Research Record 1331, 21–27.

Rix, J.R., Jacobs, L.J., Reichert, C.D., 1993. Evaluation of Nondestructive test methods for length, diameter, and stiffness measurements on drilled shafts. Field performance of structure and nondestructive evaluation of subsurface infrastructure. Transportation Research Record 1415, 69–77.

Sadri, Afshin, 2003. Application of impact-echo technique in diagnoses and repair of stone masonry structures. NDT & E International 36, 195–202.

Tong, J.-H., Wu, T.-T., Lee, C.-K., 2001. A portable transient elastic wave system for in situ nondestructive evaluation of concrete. The e-Journal of Nondestructive Testing & Ultrasonics 6 (6).

Tong, J.-H., Wu, T.-T., Lee, C.-K., 2002. Fabrication of a piezoelectric impact hammer and its application to the in situ nondestructive evaluation of concrete. Japanese Journal of Applied Physics 41 (Part 1, No. 11A), 6595–6600.

Wu, T.-T., Fang, J.-S., 1997. A new method for measuring in situ concrete elastic constants using horizontally polarized conical transducers. Journal of Acoustical Society of America 101 (1), 330–336.